Subplantation model for film growth from hyperthermal species

Y. Lifshitz,* S. R. Kasi,† and J. W. Rabalais
Department of Chemistry, University of Houston, Houston, Texas 77204-5641

W. Eckstein
Max-Planck-Institut für Plasmaphysik, D-8046 Garching bei München, Federal Republic of Germany
(Received 24 July 1989; revised manuscript received 2 February 1990)

A model describing film growth from hyperthermal ($\sim 1-10^3$ eV) species impinging on substrates is presented. The model involves a shallow subsurface implantation process called "subplantation," energy loss, preferential displacement of atoms with low displacement energy E_d, leaving the high-E_d atoms intact, sputtering of substrate material, and inclusion of a new phase due to incorporation of a high density of interstitials in a host matrix. Epitaxial or preferred orientation may result from the angular dependence of the E_d and the boundary conditions imposed by the host matrix, i.e., the "mold" effect. The discussion focuses on deposition of carbon diamondlike films, but examples of other systems, such as Si, Ge, and Ag, are provided as well. The model is supported by classical-ion-trajectory calculations and experimental data. The calculations probe the role of ion range, local concentration, backscattering coefficient, sputtering yield, and ion-induced damage in film evolution. The experimental data emphasize *in situ* surface-analysis studies of film evolution. The physical parameters of the deposition process that are treated are as follows: (i) nature of bombarding species (C^+ versus C^-, C^- versus C_2^-, $C_nH_m^+$, Ar^+, and H^+), (ii) ion energy, (iii) type of substrate, and (iv) substrate temperature during deposition.

I. INTRODUCTION

Hyperthermal species (with energy $\sim 1-1000$ eV) are used extensively in film-deposition technology in the form of plasma and ion-beam techniques for fabrication of a variety of films including metals, semiconductors, and insulators.[1–9] Among the advantages of using such species are the following: (i) epitaxial growth of crystalline films at low substrate temperatures, (ii) production of metastable phases, (iii) increased density and hardness, and (iv) excellent adhesion. Carbon-containing hyperthermal species are also widely used,[2,4,10–13] since the work of Aisenberg and Chabot,[14] for production of films with interesting properties that vary between those of the two most common carbon allotropes: graphite, the stable phase, and diamond, the metastable phase.[15]

Although extensive experimental data concerning deposition of films from low-energy species exists,[1–14] the field is characterized by insufficient fundamental understanding and little rigorous, controlled, parametric data. This is largely due to the complex chemical-physical nature of the practical deposition systems employed where the primary deposition parameters have a wide distribution of values and are difficult to define and control. The impinging species usually include a mixture of ions, free radicals, and atoms with a large spread in energy distributions and angles of incidence. Some of the processes (e.g., ion-assisted deposition) involve a complex mixture of both hyperthermal and thermal species for deposition. The pressure in most of these systems is also rather high ($>10^{-7}$ Torr). It has been recognized that parametric studies using a controlled, mass-selected ion-beam facility preferably under UHV conditions, combined with *in situ* diagnostics, is essential for the further development of the field.[16] Currently used concepts such as "preferential sputtering"[4,17] and "thermal spikes"[2,18–20] are controversial, do not provide satisfactory explanations for the existing data, nor do they assist in guiding future research. Attempts have been made to establish more rigorous models by adapting commonly used notations from the field of ion implantation.[21–28]

The present work details a subplantation (shallow implantation) model for film deposition from hyperthermal species.[29] The main focus is on the mechanisms of diamond-sp^3 film growth from carbon-containing species, but the model has a general nature and is applicable to other materials as well. Results of parametric investigations of carbon deposition conducted in our laboratory are analyzed and interpreted within the context of the model, as well as carbon and other materials deposition data from other laboratories. The analyses are supported by classical-trajectory simulations using TRIM (Refs. 30 and 31), the Biersack-Ziegler Monte Carlo program. Since the focus of this paper is on the model, the experimental procedure is not presented here but can be obtained elsewhere.[32]

This paper is organized as follows: Section II presents the supplantation model for film growth. Section III discusses the role of the deposition parameters in film growth. Section IV discusses examples of deposition of various materials from hyperthermal species. The conclusions are given in Sec. V.

II. SUBPLANTATION MODEL FOR FILM GROWTH FROM HYPERTHERMAL SPECIES

It is suggested[29] that film growth from hyperthermal species is a shallow implantation ("subplantation") pro-

©1990 The American Physical Society

cess that advances as follows.

(a) *Penetration.* Penetration of the impinging species into subsurface layers of the target. The penetration depth and distribution of the hyperthermal species in the target depend on the subplantation scheme, i.e., type and energy (E) of impinging species and nature of the target material (mass, density, chemical composition, phase, and crystallinity). Some of the impinging species may be backscattered and will not contribute to net film growth.

(b) *Stopping.* Stopping of the energetic species in the substrate via three energy-loss mechanisms:[30] atomic displacements, phonon excitations, and electron excitations. The trajectory and energy-loss processes of each projectile atom are independent of other projectiles at low fluxes. In some cases, however, e.g., high fluxes or impingement of molecules, the energy-loss processes of two or more species that simultaneously enter the same region are interdependent.

(c) *Site occupation.* The possible initial sites the impinging atoms occupy after being stopped are determined by the host matrix that serves as a "mold" for the structure to be formed. Hyperthermal species trapped in a site may occupy another site during further impingement of energetic species, either due to collisions or due to recrystallization induced by compositional changes during the deposition process. For each penetration event of an energetic species, it is the instantaneously evolving matrix that determines the site occupancy.

(d) *Phase formation.* The increase in concentration of the penetrating species in the host matrix results in the formation of an inclusion of a new phase, accompanied by outward expansion of the substrate layer (internal subsurface growth).

(e) *Surface composition.* During the early stages of film growth, the surface is mainly composed of substrate atoms due to the subsurface penetration of the impinging particles. These substrate surface atoms are gradually sputtered and/or diluted by ion-mixing mechanisms until a surface consisting of only projectile species evolves.

(f) *Film structure.* Several effects determine the phase and structure of the film: (i) The "mold" effect of the host matrix that determines the possible site occupancies of the penetrating species and places constraints on initial evolution of the new phase (i.e., the structure of an inclusion embedded in a surrounding matrix is highly influenced by the boundary conditions imposed by that matrix). (ii) Preferential displacement of atoms with low displacement energies (low-E_d) leaving atoms with high displacement energies (high-E_d) in their more stable positions. (iii) Diffusion rates of vacancies and interstitials created in the deposition process. When the temperature is sufficiently low, the interstitials are immobile and their concentration increases with fluence until an athermal spontaneous transformation to a new phase occurs.

(g) *Crystalline orientation.* Epitaxial growth and/or preferred orientation of films on crystalline materials is expected to result from the following: (i) the "mold" effect discussed in (c) and (f), (ii) the angular dependence of the displacement probability due to different E_d's needed for recoil along different crystal directions[33] (e.g., the C—C bond strength in the basal plane of graphite is 7.4 eV and is only 0.86 eV for interplanar C—C bonds[4]), and (iii) the sharply defined incident angle of the impinging species that may result in channeling along specific crystalline directions.

(h) *Sputtering.* The surface features of the evolving film and the efficiency of the deposition process depend on the sputtering yield (S) of both substrate and trapped atoms by the impinging ions. Low S is essential for efficient deposition and is necessarily less than unity for net film growth to occur at all.

(i) *Film evolution.* Evolution of a pure film from hyperthermal species impinging on a substrate consisting of atoms different from that of the bombarding species is feasible only when collisional ion mixing and diffusion processes are small enough, so as to allow evolution of a pure layer. In this case the "deposition" process has two stages: (i) initial "heterodeposition" followed by evolution into a pure layer as described in (a)–(e) and (ii) "homodeposition" of energetic species adding to the pure film.

Some of the steps presented above are preliminary, and further rigorous theoretical treatment is needed. Atomistic calculations of phase evolution of a subplanted material in a host matrix are needed for further development of the "mold" effect. A simulation program that treats crystalline materials, rather than amorphous structures as used herein, is necessary for further development of the details of epitaxial growth.

III. ROLE OF PARAMETERS IN FILM GROWTH: CARBON SUBPLANTATION

A. Introduction and basic assumptions

Calculations of ion penetration into different substrates are needed for evaluation of the physical phenomena involved. TRIM (Refs. 30 and 31) calculations were performed assuming (a) an amorphous material, (b) a binary collision approximation, and (c) independent uncorrelated trajectories. Chemical reactions and diffusion are neglected. Comparison between TRIM calculations and more sophisticated programs that consider many-body interactions and bonding effects shows differences only at very low energies, e.g., $E<10$ eV for H;[28] hence the present calculations should be valid for the energy range investigated (typically 100–1000 eV). The calculated physical quantities include (i) range of species (R_p), (ii) distribution profile [proportional to range straggling $(\Delta R_p)^{-1}$], (iii) backscattering yield (Y_{BS}), (iv) sputtering yield (S), (v) damage [number of displacements per impinging ion (N_d)], and (vi) relative importance of energy-loss channels (displacements, phonon excitation, and electron excitation).

The calculations were performed for different projectiles (CH, H, and Ar) impinging on different noncarbon substrates (Li, Si, Ni, and Au) or a specific carbon allotrope (graphite or diamond). Experimental values of physical parameters were used whenever available. Most calculations were performed under the assumption of a low fluence, i.e., the dynamic evolution of the composi-

tion of the target due to incorporation of species during bombardment is neglected. The actual programs that were used are TRIM (Ref. 30) versions two (for R_p, Y_{BS}, and N_d) and four (for S) that use the universal [Ziegler-Biersack-Littmark (ZBL)] potential and assume that the electronic energy loss is nonlocal, i.e., independent of the specific atomic collisions (Lindhard-Scharff approximation). Some dynamic calculations were performed using the TRIDYN Version-32 program of Möller *et al.*[34] with the Kr-C interaction potential. The inelastic electronic energy-loss function is an equipartition between the nonlocal Lindhardt-Scharff and the local Oen-Robinson model. The purpose of these more time-consuming calculations was to evaluate the evolution of the subplanted layers and to study the change of some physical quantities (S and Y_{BS}) associated with the subplantation process.

Hyperthermal species-target interactions leading to film evolution can be characterized by three distinct time scales:[28]

(i) A collisional stage in which the hyperthermal species transfers its energy to the target atoms ($\sim 10^{-13}$ sec).

(ii) A thermalization stage in which the energetic atoms participating in the collision cascade lose their excess energy to reach thermal equilibrium with the surrounding atoms ($\sim 10^{-11}$ sec).

(iii) A long-term relaxation stage ($\sim 10^{-10}$–1 sec) in which the final structure of the material is determined.

The first stage is characterized by processes such as displacements, sputtering, and incorporation of interstitials; it is treated by TRIM (Refs. 30 and 31) calculations. The second stage is less understood and is often described in "thermal spike"[18–20] notations. The third stage is governed by processes such as diffusion of vacancies and interstitials, phase transformations, and chemical reactions. It is assumed, as a first approximation, that the thermalization stage has a second-order effect on film evolution and that the excess energy of atoms excited in the first stage is distributed within the target, leaving the atoms in positions determined in stage (i).

B. Fluence dependence of film evolution: Subsurface nature of process

Auger-electron spectroscopy (AES) of films deposited from C^+ ions show[13,29,32] (i) an almost constant substrate AES intensity initially with an associated almost linear increase of the C AES intensity, followed by a sharp decrease of the substrate intensity at a high C^+ fluence (Fig. 1) and (ii) an initial substrate–C-compound phase (AES line shapes typical for carbides) that in some cases evolves to a graphitic stage and then to a diamondlike stage (Fig. 2). Typical surface-deposition processes [three-dimensional (3D) island (Volmer-Weber growth), 2D layer-by-layer (Frank–de Marwe growth), or a combination of both (Stranski-Krastanov growth)] are characterized by an initial rapid decrease of the substrate AES intensity (dashed curve in Fig. 1).[35–37] The initial constant substrate AES intensity during C^+-ion impingement and the C *KLL* AES intensity increase are characteristic of a subsurface process. This is consistent with

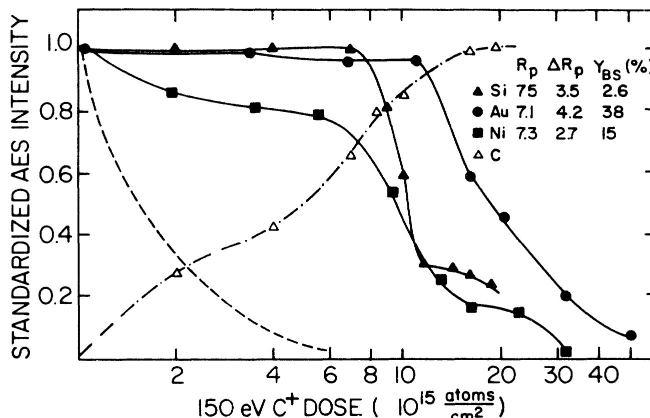

FIG. 1. Substrate AES peak intensities (solid lines) as a function of 150-eV C^+ ion fluence at normal incidence. Ni (61 eV), Si (92 eV), and Au (69 eV) AES transitions are used. The peak intensities are normalized to that of the clean surface. The dashed line corresponds to Si AES intensity as a function of thermally evaporated Ge dose (Ref. 35). The dashed-dotted line corresponds to the carbon *KLL* AES peak intensity specifically for the Si host. TRIM results include R_p, projected range (10^{15} atoms/cm^2); ΔR_p, range straggling (Å); and Y_{BS}, backscattering yield.

the subplantation model, where the C^+ ions penetrate into subsurface layers (the calculated $R_p \sim 10$ Å) and prolonged carbon impingement is needed for removal of the substrate surface atoms by sputtering and/or dilution by ion mixing. Figure 2 correlates the evolution of the carbon phases and AES line shapes with the local concentration of carbon atoms. The evolution of the initial carbide phase is due to penetration of carbon *into* the substrate matrix (M), forcing the formation of C—M bonds (a carbide) even in cases where stable carbides are not known, e.g., Au. A further increase in the C^+ fluence may result in an increased local carbon concentration that forms a 2D carbon layer (graphiticlike). Higher C concentrations form a 3D bulk-carbon phase—graphite or sp^3 diamondlike, depending on the deposition scheme. Dynamic TRIM calculations of C^+ impingement on Au, for example, demonstrate (Fig. 3) the stages of subplantation growth: (i) Penetration of C into subsurface layers, (ii) increase of the local C concentration of subsurface layers, leaving a "skin" of gold surface atoms, (iii) sputtering and dilution of the gold surface atoms until a pure C layer is formed, and (iv) growth of a pure C matrix. An interesting effect of the substrate on the evolution of the subplanted film is shown in Fig. 4. The initial Y_{BS} of C^+ from the heavy Au atoms is high and the resulting sputtering yield S of the C atoms (after a significant amount of C was deposited) is also high. Evolution of the C layer and decrease in the near surface concentration of Au atoms is associated with a decrease in Y_{BS} and S of the carbon.

C. C^+ energy dependence of film evolution preferential displacement

TRIM calculations were performed for C^+ impinging on different materials in the range 10 eV to 10 keV (Fig.

5). The relevant physical quantities include (i) R_p, (ii) ΔR_p, (iii) Y_{BS}, (iv) S, and (v) damage (N_d). R_p determines the amount of substrate atoms that must be removed before a pure C layer is formed. ΔR_p determines the minimum fluence needed for formation of a C inclusion (the maximum local concentration is proportional to ΔR_p^{-1}). Y_{BS} and S determine the efficiency of the deposition process. N_d determines the phase and structure of the evolving film. Successful pure C film depositions involve small R_p, low ΔR_p (high local concentration), low S and Y_{BS}, and controlled N_d, dictating an optimal energy region for deposition.

Of special interest to the mechanism of film growth are S and N_d. Preferential S of amorphous carbon and graphite constituents, leaving the diamond constituent undisturbed, has been suggested[4,17] as a mechanism for diamond growth from hyperthermal species. Reported

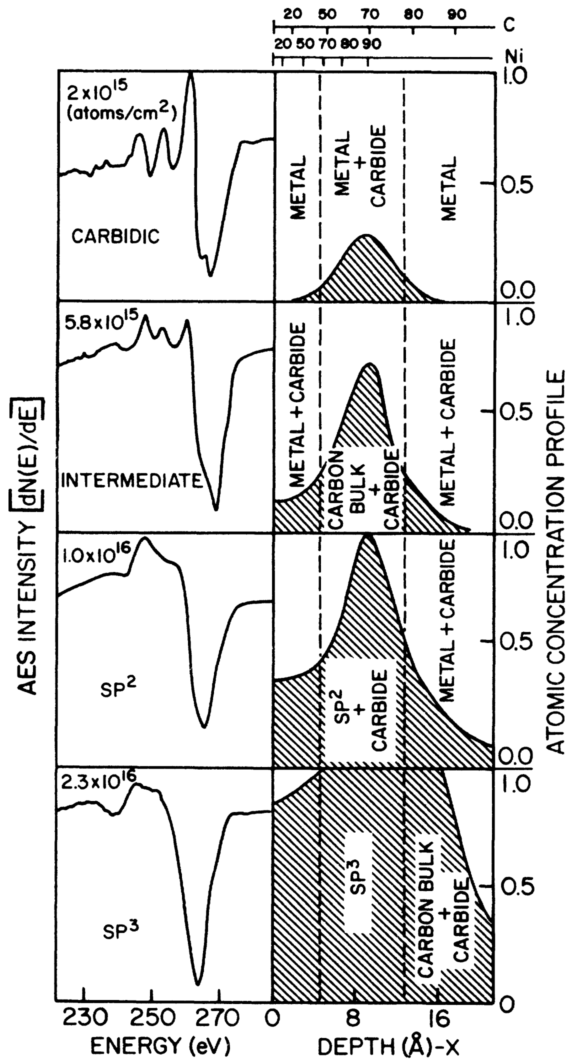

FIG. 2. Stages of subplantation growth. Left column: C KLL AES line shapes for different C^+ fluences for 150-eV C^+ ions on Ni(111). Right column: subsurface entrapment of energetic carbon and buildup of carbon deposits. The top scale indicates the relative contribution to the AES intensity (%) derived from a layer of depth x (lower scale).

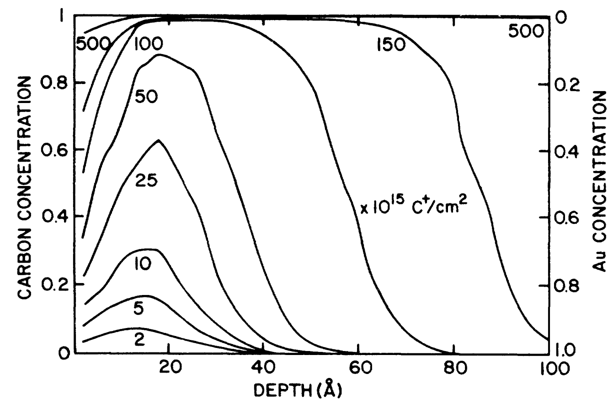

FIG. 3. Dynamic TRIM (TRIDYN Version-32) (Ref. 34) calculations of evolution of C concentration with fluence from 150-eV C^+ ion impingement on Au. The fluences are given in $\times 10^{15}$ C^+/cm^2. Note the subsurface entrapment of the C^+ and the high fluence needed to remove the Au surface layer.

experimental results[38] indicate differences in the surface binding energy (SBE) of C atoms in different allotropes. TRIM calculations can be fitted to these results (Fig. 6) if we assume a SBE of 3.5 eV for graphite and a SBE of 2.0 eV for an evaporated C film, rather than a SBE of 7.4 eV (heat of sublimation of graphite and diamond). This may be due to weaker C atom-surface bonding for specific films. Nevertheless, both the calculated and experimental[38] S of graphite and amorphous carbon by C^+ and Ar^+ (Fig. 6) are extremely low at a normal angle of incidence so that preferential sputtering can only play a minor role in enrichment of the sp^3 component. On the

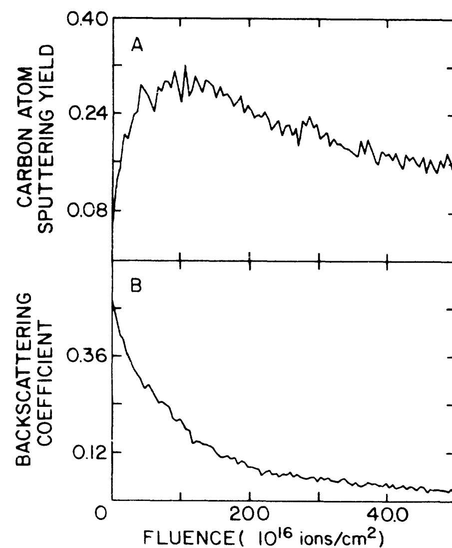

FIG. 4. Dynamic TRIM (TRIDYN Version-32) (Ref. 34) calculations of C sputtering yield (S) and backscattering coefficient from 150-eV C^+ ion bombardment of Au. Note initial increase of S due to C incorporation to reach a maximum value enhanced by backscattering from the Au atoms. The initially high backscattering (due to Au) decreases as the Au atoms are sputtered and diluted and a pure carbon layer evolves (Fig. 3).

other hand, the marked difference in the experimental E_d's (Ref. 4) between graphite (25 eV) and diamond (80 eV)[39] suggest preferential displacement of low-E_d (graphitic or amorphous carbon) atoms leaving the high-E_d (diamond) atoms in their more stable positions. TRIM calculations indicate (Fig. 7) that in the energy region of 100–200 eV, for example, $N_d = 0.75-1.7$ for graphite and only 0.03–0.3 for diamond. At higher energy the N_d's for diamond are still $\sim\frac{1}{3}$ those of graphite, but both are high ($N_d > 1$), resulting in significant damage in both cases. Experimental results[32,40] of C deposition from hyperthermal species indicate optimal deposition of films

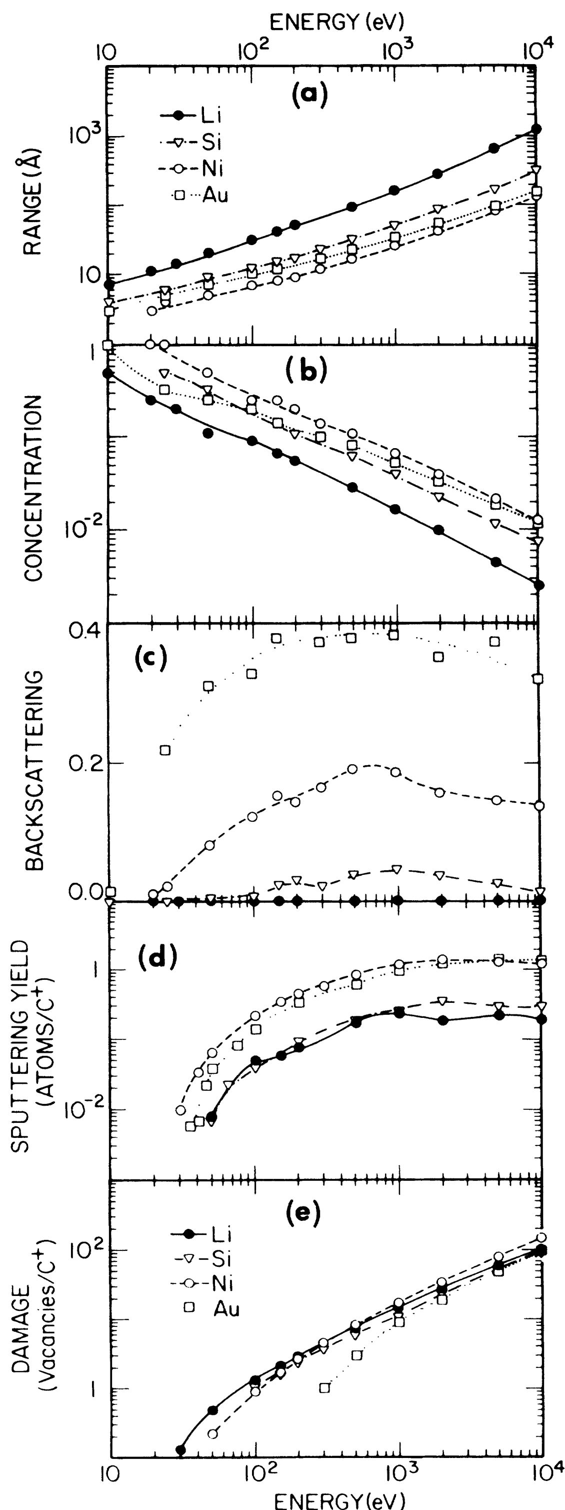

FIG. 5. TRIM calculations of C bombardment of Li, Si, Ni and Au. (a) Range (R^P), (b) local concentration ($1/\Delta R_p$: ΔR_p, straggling), (c) backscattering Y_{BS}, (d) sputtering yield (S) of target atoms, and (e) damage (N_d, number of displacements per impinging ion). Note significant mass effects on R_p and Y_{BS}.

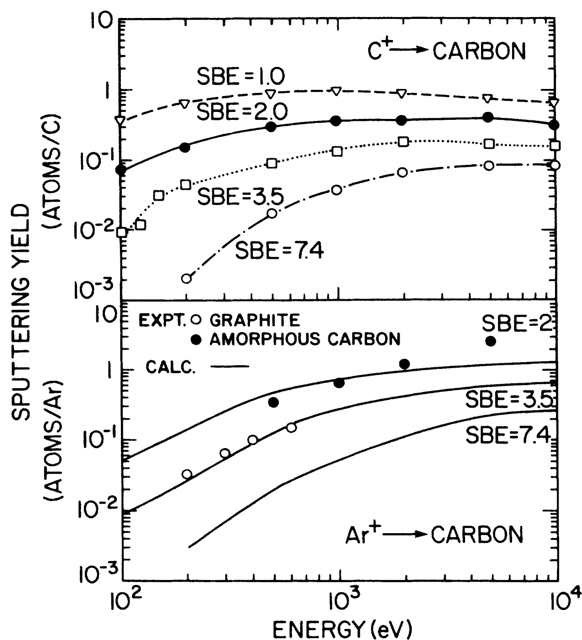

FIG. 6. TRIM calculations of S of carbon for different C^+ and Ar^+ energies and surface binding energies (SBE). The S is sensitive to the surface binding energy (SBE). The choice of the proper SBE for different carbon forms was made by comparison to experimental results (Ref. 38) of carbon bombardment with Ar^+ (Ref. 38). For C^+ on carbon (upper figure) the symbols represent calculated data points through which the lines were interpolated. For Ar^+ on carbon (lower figure) only experimental data points are given while the lines were fitted to the calculated data.

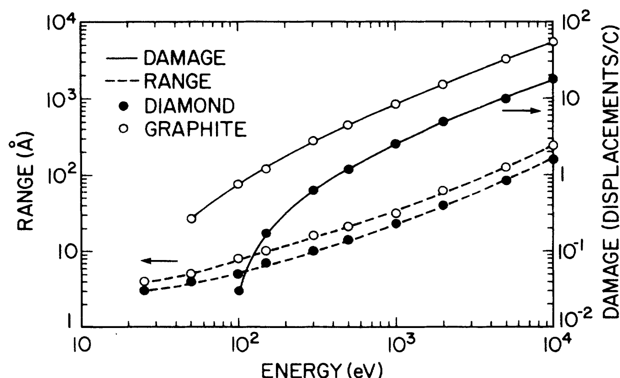

FIG. 7. TRIM calculations of N_d and R_p for C^+ ions with $E = 10$ eV to 10 keV impinging on graphite ($E_d = 25$ eV, density $= 2.26$ g/cm^3) and diamond, ($E_d = 80$ eV, $d = 3.5$ g/cm^3). Note preferential displacement of graphite compared to diamond, especially for $E = 100-200$ eV, where N_d(diamond) $\ll 1$.

with the sp^3 short-range order in the energy range of ~60–200 eV and maximum density in the energy range of 100–200 eV.[41] At higher energy (~500–1000 eV), deposition of amorphous carbon was reported[4,41–45] due to the large amount of damage (N_d=4.2–8.4 for graphite and N_d=1.2–2.6 for diamond) induced. Higher fluences are needed to form pure C layers at such high energy due to the relatively high R_p and ΔR_p. At lower energy (<60 eV) the damage for all constituents is low and little displacement occurs. At very low energy (<10 eV) the penetration depth of the C^+ becomes negligible and the subplantation aspects no longer exist; graphitic films similar to those deposited from thermal species are formed.

Figure 8 summarizes the effects of energy on carbon film deposition. At low energy (but high enough to trap carbon in subsurface layers), no displacement occurs and C is trapped as interstitials. A high concentration of interstitials is formed when the C^+ fluence increases. An athermal, spontaneous precipitation[44] of a new phase is expected. The formation of a diamond (sp^3) constituent may be favored by the "mold effect" and by the highly excited environment due to electronic and phonon excitations (sometimes referred to[18–20] as "thermal spikes"). High concentrations of interstitials can also induce stress[43] equivalent to static pressures of ~10–100 kbar, favoring the formation of metastable phases.

At medium energy the preferential displacement mechanism is effective, favoring the formation of diamond-sp^3 inclusions and reducing the amount of graphitic constituents. At still higher energy the damage is high for all constituents resulting in an amorphous material of sp^n (n=1–3) hybridizations.[4]

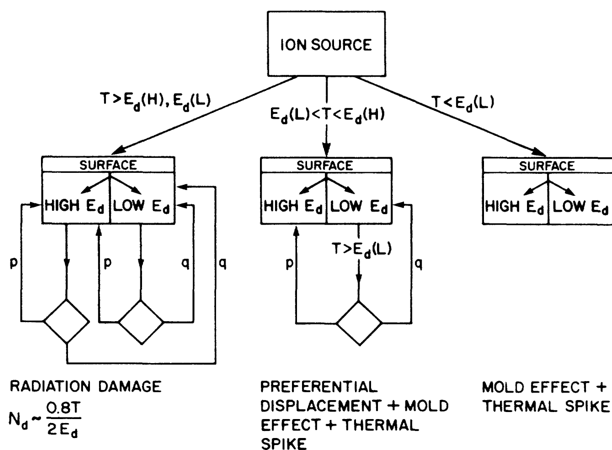

FIG. 8. Schematic illustration of dense matrix formation for three energy ranges: (i) $T<E_d(L)$, only "mold effect"; (ii) $E_d(L)<T<E_d(H)$, preferential displacement; (iii) $T>E_d(H)$, radiation damage and amorphization. E_d, displacement energy; H and L, high- and low-E_d components; T, energy transferred in collision by primary ion; N_d, number of displacements per incident primary particle p; q, probabilities of high- and low-E_d atomic-site occupancies.

D. Angle of incidence (α)

Several factors such as R_p, ΔR_p, Y_{BS}, and S are sensitive to the angle of incidence α of the impinging species (angle between beam and surface normal). Shallower subplantation is expected for impingement at glancing angles. Y_{BS} is enhanced at glancing α, especially for those cases where no backscattering is possible in a single collision. This enhanced Y_{BS} also increases the S of the different C phases (Fig. 9); this S is low at normal α. The trajectories of the penetrating species are dependent on the target crystallographic orientation and α, thereby determining the C distribution in specific sites. The N_d and relevance of the preferential displacement mechanism are also sensitive to α due to different E_d's needed for recoiling of atoms along different crystallographic directions.[33] Impingement at grazing α is also associated with a large velocity component parallel to the surface that enhances surface mobility and may contribute to surface rather than subsurface deposition.[28]

E. Role of substrate material

The formation of a pure film necessitates a shallow implantation range, low S and Y_{BS}, and low intermixing between projectile and target atoms. Si, Ni, and Au have similar ranges for C deposition at 100–200 eV (Figs. 1 and 5). The difference is the high (~40%) Y_{BS} of C^+ from Au due to its large mass, compared to ~1–3%

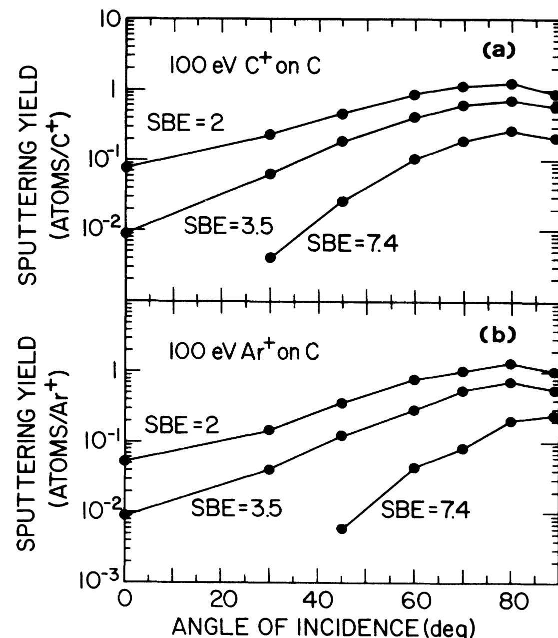

FIG. 9. TRIM calculations of angular dependence of S for (a) 100-eV C^+ ions and (b) Ar^+ ions on diamond, graphite, and amorphous carbon. Note that there is no case where $S\sim1$ for both graphite and a-C and $S \ll 1$ for diamond (conditions needed for efficient sp^3 enrichment from "preferential sputtering"). Choice of the SBE for graphite (3.5 eV) and amorphous carbon (2 eV) was made by comparison to experimental results of Ar^+ bombardment (Ref. 38). For diamond the heat of sublimation (7.4 eV) was used.

from Si and ~15% from Ni. The decrease of the metal AES intensities shows (Fig. 1) that the C^+ fluences needed for pure carbon layer formation (i.e., disappearance of the metal AES lines) is ~60% higher for Au than for Ni and Si, in agreement with the trapping efficiencies $(1-Y_{BS})$. Another difference is the higher S of Au and Ni [~30%, compared to ~10% for Si (Fig. 5)] due to the lower heat of sublimation of the metals and the higher efficiency for C backscatter from Au and Ni, resulting in recoiled Au and Ni atoms from backscattered C atoms. The higher Y_{BS} from Au compared to Ni is compensated by the much lower energy transferred (T) to the high-mass Au atoms in each collision so that S of Ni by C^+ is slightly higher than that of Au. The low T for Au also results in lower damage (Fig. 5) to the Au compared to Si and Ni [N_d(Au, 150 eV)~0.4, N_d(Si, 150 eV)~1.7, N_d (Ni, 150 eV)~1.7].

Li is different from the previous substrates because R_p, ΔR_p, and N_d are significantly higher than on Ni, Si, and Au. The behavior of Li in a C^+-bombarded target was investigated using a $Cu_{0.8}Li_{0.2}$ alloy whose surface composition could be changed to $Cu_{0.1}Li_{0.9}$ by annealing and to $Cu_{0.6}Li_{0.4}$ by Ar sputtering of the annealed sample (as determined from AES). Impingement of 150-eV C^+ ions on a ~90% Li surface results [Fig. 10(a)] in the formation of lithium carbide (revealed by a chemical shift of the Li *KVV* AES line from a metallic to ionic position[46,47]) with no evolution of a pure carbon layer, even at fluences of 10^{17} C^+/cm^2, i.e, ten times greater than that needed for Ni, Si, or Au. One reason for this is the broader distribution profile, which suggests that the fluence needed is three times larger than that in Ni or Si. Bombardment of Li with 30-eV C^+ ions [Fig. 10(b)], however, produces similar results, i.e., no evolution of a pure C phase even at a fluence of 10^{17} C^+/cm^3. At this energy the C^+ range in Li is similar to that of 150-eV C^+ ions in Ni, Si, and Au and the straggling is ~40% lower. C-Li intermixing due to collisional effects and Li diffusion are most likely the reason for the lack of film evolution, as is also indicated by surface analysis that shows both surface Li and C with ionic Li AES line shapes and a C AES line shape of lithium carbide. The shift from elemental to ionic Li is complete for 30-eV C^+ ions and only partial for 150-eV C^+ ions, possibly due to the deeper penetration of the 150-eV C^+ ions leaving a Li layer on the surface. Measurements on the $Cu_{0.6}Li_{0.4}$ surface, where R_p and ΔR_p are only slightly higher than the other substrates, produced similar results.

Synergistic effects of specific C-substrate combinations must be considered. Y_{BS} and S from C^+ impinging at normal incidence on graphite and diamond are extremely small ($Y_{BS} < 10^{-3}$ and $S < 0.10$ for $E < 1$ keV). C^+ can backscatter efficiently from high-mass substrates, resulting in enhancement of S and reduction of the initial net deposition efficiency. For example, Table I gives the calculated enhancement factor of S in a 50% AuC alloy compared to a pure C target bombarded with C^+ ions. The specific crystalline environment of the target determines the possible final sites of the penetrating species and also affects the phase and structure of the evolving inclusion by imposing constraints on its evolution (a "mold" effect). In the initial stage of deposition prior to the formation of a new phase, this may lead to a correlation between the interface layer and substrate. Upon further deposition, the evolving film may be oriented[17,40] or grow epitaxially. The most favorable matrix for epitaxial growth of a diamond film is that of diamond, i.e., homoepitaxial growth.[48]

F. The role of substrate temperature

Two different issues are associated with substrate temperature effects on C film deposition: (i) The thermal stability of the final film including the film-substrate interface and (ii) the evolution of the C phase on a substrate held at a specific temperature.

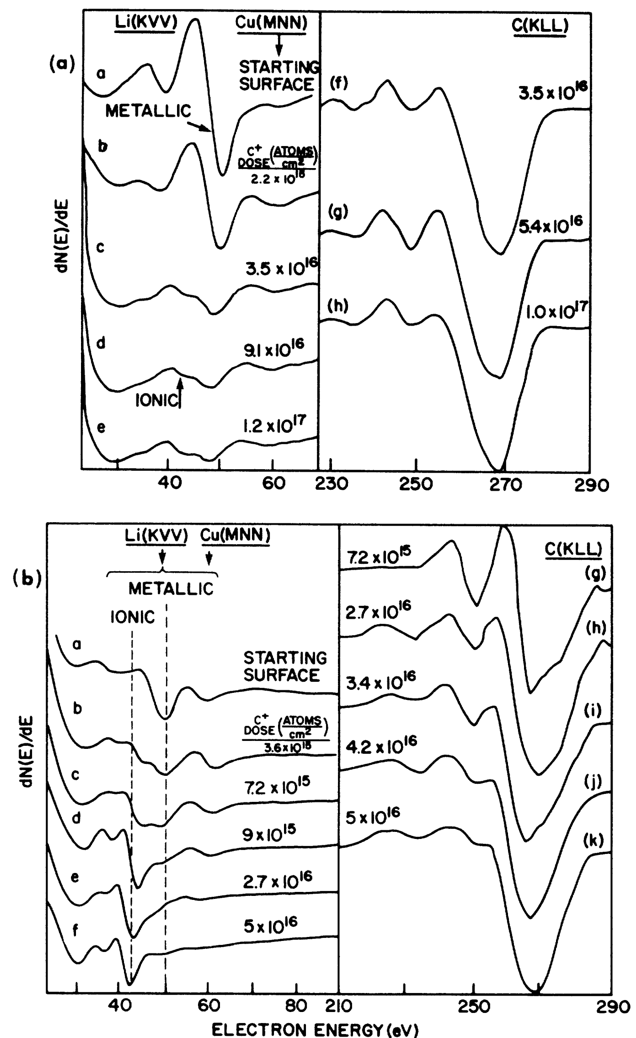

FIG. 10. Stages of film evolution on Li (surface-enriched CuLi alloy) following (a) 150-eV C^+ and (b) 30-eV C^+ ion bombardment. Evolution of the C *KLL* (right) AES line shapes indicates Li-C formation and no graphite or diamond formation for the fluences studied. Evolution of the Li(*KVV*) (left) line shapes indicates full transformation from metallic to ionic Li (Refs. 46 and 47) for 30-eV C^+ ion bombardment and partial transformation from metallic to ionic Li for 150-eV C^+ ion bombardment. Note that 150-eV C^+ ions penetrate deep into the Li and some surface Li remains metallic.

TABLE I. TRIM calculations of the enhancement factor (EF) of the sputtering yield due to a Au substrate. The EF is the ratio of the sputtering yield of $Ar^+ \rightarrow AuC$ (50%:50%) to $Ar^+ \rightarrow C$ for the different carbon allotropes, diamond, graphite, and amorphous C. The EF is calculated for different energies and different angles of incidence. The EF is large for small C sputtering yields ($S<0.1$) and small for large C sputtering yields ($S>0.1$). An EF of <1 reflects the lower concentration (50%) of carbon in the Au-C alloy compared to a pure carbon layer. SBE denotes surface binding energy.

		Enhancement factor (EF)		
E (eV)	α	Diamond (SBE, 7.4 eV)	graphite (SBE, 3.5 eV)	a-C (SBE, 2 eV)
100	0°	>38.0	12.9	3.6
	45°	12.8	1.9	1.0
	60°	2.5	1.1	0.70
200	0°	31.3	7.9	2.5
	45°	2.9	1.25	0.72
	60°	1.3	0.71	0.56

Carbon films with different sp^3-to-sp^2 ratios tend to graphitize when annealed to temperatures higher than 400 °C.[2,4,10] This tendency is accelerated when some interdiffusion between the C layer and substrate exists. Carbon films on Ni are unstable upon annealing due to C diffusion into the bulk, while a small decrease of the C concentration is observed on Si and no C diffusion into the substrate was detected on Au, even at 900 °C (Fig. 11).

The carbon phase is sensitive to the temperature of the substrate upon which the C^+ species impinge.[49,50] While a film with sp^3 short-range order evolved at 70 °C and below on Ni, sp^2 films evolved at 100 °C and up. Graphitization occurred even in the regions of 100–400 °C where the sp^3 diamondlike films were stable under post-deposition annealing. This phenomenon is surprising since the energy associated with the different temperatures is negligible (<0.1 eV) compared to the energy of the C^+ (~ 100 eV). The result may be due to the temperature dependence of the mobility of vacancies and C interstitials.[51–53] While the vacancies are mobile only at high temperatures (400 °C and up), the interstitials become immobile only at room temperature and below. It is thus suggested that at temperatures lower than 70 °C, impingement of low-energy C^+ creates immobile carbon interstitials. Their concentration increases with fluence, creating stress in the matrix.[45] At a certain stage spontaneous athermal transformation to a dense sp^3 phase occurs. A similar effect of spontaneous athermal transformation initiated by helium interstitials has been observed.[44,45] At temperatures exceeding 100 °C, the C interstitials are mobile and migrate to the surface on which they can form sp^2 layers.

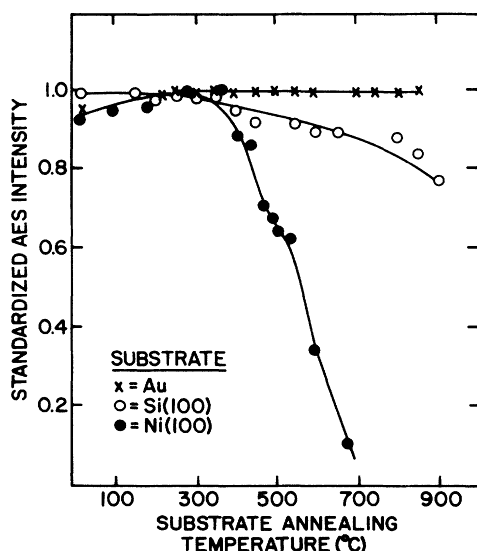

FIG. 11. Temperature stability of $\sim$75-Å-thick carbon films deposited on Au, Si(100), and Ni(100) revealed by the C(KLL) AES intensity of the films. The substrate was maintained at the temperature indicated in the figure for 2 h prior to the measurement.

A different temperature effect exists during C^+ impingement on a diamond surface. Successful diamond deposition has been observed at a diamond target temperature of 700 °C, where the vacancy mobility is high enough to account for the annealing of the damage created by the 900-eV C^+ ions.[48] Internal diamond growth occurs, similar to that reported for high-energy ($\sim$50-keV) C^+ ion impingement.[54] The obvious driving force for the metastable diamond formation is the "mold" effect of the diamond host matrix that favors the inclusion of diamond to that of graphite.

According to the "thermal-spike" model,[18–20] the dense phase evolves during the short period ($\sim 10^{-11}$ sec) of local excitation resulting from projectile energy loss. Since the energy associated with substrate annealing from room temperature to $\sim$100 °C is negligible ($\sim$0.01 eV) compared to that associated with the "thermal spike" ($\sim$10–100 eV), it is expected from "thermal-spike" considerations that the evolution of a dense sp^3 C phase will be temperature independent as long as the films are stable upon post-deposition annealing, i.e., at least $T<400$ °C. This is in contradiction with the experimental results.

G. Role of the type of the carbon-containing species

Different C-containing hyperthermal species have been used for C deposition including C^+, C^-, C_2^-, and $C_nH_m^+$.[2,4,12–14,17,32,40–43,48–50,54,55] Other hyperthermal species (i.e., Ar^+ and H_2^+)[2,4,14,56] have also been used simultaneously with C-containing species in order to modify film properties. An impinging hyperthermal molecule is neutralized upon approaching a surface.[57] If its energy is sufficient ($\sim$ a few tens of eV), it dissociates upon penetration into its atomic constituents, each of which possesses an energy $(m/M)E$, where m is the mass of a constituent atom and M the mass of the molecule.

1. Role of C_n species ($n>1$)

The simplest case is the comparison between C^- and C_2^- impingement. Bombardment by 200-eV C_2^- ion may be regarded as equivalent to 100-eV C^- ion impingement with the fluence increased by a factor of 2. The maximum density of diamondlike films has been achieved with 100–200-eV C^- ions and $\leq$100-eV C_2^- ions.[41,55] This discrepancy may be due to the differences in the subplantation process between C_2^- and C^-. At practical current densities (≤ 10 mA/cm^2), each single trajectory is independent of previous and following trajectories due to the short ($\sim 10^{-11}$ sec) relaxation periods of the excited atoms along the trajectory. This is not the case for the penetration of correlated fragments of a molecule. It is, however, logical to assume that each fragment moves in a matrix excited by the other fragments resulting in a virtual matrix with reduced displacement and binding energies. The maximum density for films deposited from C_2^- is therefore achieved at a lower energy of each C atom than for C^-.[41,55] This argument can be extended to include cluster deposition (C_n^+), provided that the energy of each fragment is sufficient to penetrate into subsurface layers.

2. Role of charge

The optimal energy for deposition of a dense carbon matrix was found to be identical for both C^- and C^+ ions.[13,31,41,55] Ions approaching a surface are neutralized[1,57] by excitation processes in the surfaces that depend on the ion-surface system. The magnitude of the differences between the effects of C^+ and C^- bombardment of surfaces can be evaluated from the energy difference between these two electronic configurations that is of the order of 10 eV. This is small compared to the ion energy of 100 eV and is even less than the energy spread of the C^- beam.[41,55] No significant charge effect on deposition is thus expected for bombardment with $\sim$50–1000-eV ions. This does not refer to the practical problem associated with deposition from charged species such as charging of insulating targets.

3. Role of Ar species

Ar^+ is often used simultaneously with thermal or hyperthermal C species for C deposition.[2,4,14] While Ar induces collisional effects (Fig. 12) similar to those of hyperthermal C species with slightly higher N_d and S, it contributes no C atoms to the evolving film and it is entrapped in the evolving matrix-inducing stress and damage. In order to investigate the role of Ar in C deposition, graphitic films were bombarded with low-energy Ar^+ ions; no evolution of the graphitic film to a diamond-sp^3 stage was detected, as occurred for similar bombardment of the same film with C^+ ions. Ar^+ bombardment, however, resulted in significant Ar entrapment as detected by AES. It has been suggested that Ar^+ bombardment preferentially sputters amorphous carbon and graphitic constituents with little effect on the diamond constituent.[4,17] Since the S of carbon by Ar^+ ions at normal incidence angles is extremely small in the region of $\sim$100 eV, Ar^+ beams at least ten times more intense than the C^+ beams are needed to efficiently sputter the amorphous carbon and graphitic constituents. Ar entrapment is, however, expected under these conditions, damaging the evolving film. Moreover, Ar^+ bombardment of a diamondlike film at an energy of $\sim$3 keV and incident angle of 60° resulted in graphitization. In many cases Ar^+ bombardment of carbon films is performed at glancing angles, but the necessary S for efficient preferential sputtering of carbon films to form diamond is not obtainable (Fig. 9).

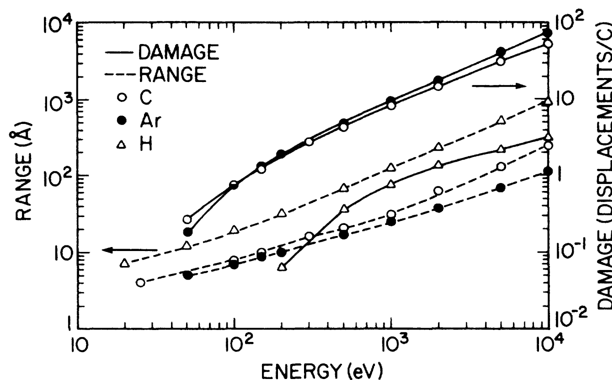

FIG. 12. TRIM calculations for H^+, Ar^+, and C^+ subplantation onto graphite (density 2.26 g/cm^3, $E_d=25$ eV). Note similar R_p and N_d for Ar^+ and C^+ ions, and high R_p and low N_d for H^+ ions.

4. Role of hydrogen

Hydrogen plays an essential role in chemical-vapor deposition (CVD) diamond film deposition by preferentially etching graphitic and amorphous carbon constituents.[11,58] High hydrogen concentrations (e.g., $>99\%$ H_2, $<1\%$ CH_4), high substrate temperatures, and an excitation source for dissociation of the H_2 molecule to provide atomic-hydrogen spieces are required. The role of hydrogen in the stabilization of the diamond surfaces by terminating "dangling bonds" is also important.[10,11,58] These concepts are often adopted for carbon deposition from hyperthermal species. TRIM calculations of hydrogen penetration into carbon show (Fig. 12) high R_p, low N_d, and low S ($<10^{-2}$), with the main energy-loss mechanism being electronic excitation. Hyperthermal hydrogen bombardment is expected to be associated with large

hydrogen concentrations in the carbon layer. Bombardment of graphitic films that were previously exposed to Ar^+ ions with 30-eV D_2^+ ions showed two interesting phenomena: (a) amorphization (revealed by a change in the C *KLL* AES line shape) and (b) removal of the Ar (revealed by the disappearance of the Ar AES signal). The amorphization may be associated with ionization processes in the graphitic film and C-H formation. The removal of the Ar may be due to *chemical sputtering* of C by low-energy hydrogen,[59] thus enhancing the collisional sputtering (which is very small).

5. *Role of hydrocarbon species*

Impingement of hydrocarbon species is a complex phenomenon even with controlled and well-defined mass, energy, and α. The following points can be drawn from TRIM calculations and the subplantation model.

(a) Impingement of low-energy hydrocarbons, where the energy is insufficient to dissociate the molecule, results in deposition of a hydrocarbon film.

(b) Higher-energy impingement of C_mH_n molecules results in complete dissociation to the C and H constituents. The C energy is $12E/12m+n \sim E/m$, while the H energy is 12 times lower, i.e., $E/12m+n$ (neglecting the partition of the internal energy of the molecule).

(c) The trajectories of all of these species are interdependent, causing lower effective E_d in the target material as described previously for C_n.

(d) The low-energy hydrogen can be trapped (forming hydrogenated-amorphous carbon *a*-C:H), reflected, or can chemically etch the evolving carbon layer.

(e) The R_p of the penetrating C atoms is higher than those of the H atoms due to the high energy of the C atoms (see Table II). At low CH_4^+ energy, for example, the difference between the profiles is minor. The difference is significant for higher energy (e.g., >200 eV), resulting in a dense carbon layer (with low hydrogen concentration) at the deepest R_p, while the outermost surface layers have a high concentration of hydrogen. Some of this hydrogen is released when the local hydrogen concentration exceeds saturation values of $\sim 50\%$.[59] Moreover, these hydrogen rich layers are also physically sputtered by the hyperthermal fragments and chemically sputtered by the low-energy hydrogen atoms, resulting in the formation of dense carbon films with little hydrogen. Other phenomena that assist in the formation of a dense carbon film with low hydrogen concentration at CH_4^+ $E>200$ eV are the preferential displacement of H atoms, leaving the C atoms at their positions, and preferential C—H bond breaking and hydrogen release. The hydrogen concentration may however be dependent on the abundance of H^+ and H_2^+ species in the system that have a higher range than the C^+ species with the same energy.

These phenomena explain the energy dependence of film deposition from hyperthermal hydrocarbons,[4] namely (i) hydrocarbon film formation at low energy; (ii) *a*-C:H films at higher energy; (iii) dense carbon formation (with small hydrogen concentrations) at still higher energy.

IV. HYPERTHERMAL SPECIES DEPOSITION OF OTHER MATERIALS

Subplantation is a general model that is applicable to other materials besides carbon. Some examples will be presented in this section in order to demonstrate the generality of the approach. Direct ion-beam deposition will be considered first followed by the more complicated system of ion assisted deposition.

A. Mass-selected ion-beam deposition (MSIBD)

Deposition from mass-selected low-energy ion beams of Si, Ge, and Ag onto Si has been studied by several groups.[7,21,22,60–64] In these cases, the mass of the impinging ion is heavier than that of C, resulting in high S and N_d. The results can be summarized as follows: (i) epitaxial growth was obtained at lower substrate temperatures (~ 400 K for Ge and Si and room temperature for Ag) than those needed for surface-deposition techniques such as CVD and MBE, (ii) defects were found particularly at low temperatures, e.g., room temperature, where amorphous Ge and Si films were reported, and (iii) limited use of trajectory calculations was reported.

TRIM calculations provide information on the evolution of the subplanted layers (Figs. 13 and 14). The subsurface nature of the process is evident from the range of the ions, even at $E \sim 40$ eV ($R_p = 5-9$ Å). Subplantation into Si is associated, for all these cases, with low S ($S \leq 0.08$ for $E \leq 200$ eV and $S \leq 0.25$ for $E \leq 500$ eV) so that net deposition occurs. When a new layer is formed, the energy transfer T to the Ge, Ag, or Au target atoms becomes much more efficient than for Ge, Ag, and Au energy transfer to Si target atoms, resulting in much higher S (0.26 for 200-eV $Ge^+ \rightarrow Ge$ ions, 0.88 for 200-eV $Ag^+ \rightarrow Ag$ ions, and 0.53 for $Au^+ \rightarrow Au$ ions), thus lowering the energy regions for efficient deposition to $E<100$ eV. The radiation damage is significantly higher in these systems than for $C^+ \rightarrow$graphite and diamond. The $N_d > 0.6$ and >1.7 for $E=50$ and 100 eV, respectively. BS of the impinging ions for all of these cases is very low, so that the deposition efficiency is mainly determined by S.

TABLE II. TRIM Calculations of the distribution of H and C in carbon following bombardment with CH_4 ions. E_i, energy (eV) of species i ($i = CH_4$,C,H); R_i, range (Å) of species i; ΔR_i, range straggling (Å) of species i.

E_{CH_4}	E_C	R_C	ΔR_C	E_H	R_H	ΔR_H
100	75	6	2	6.25	3	<1
200	150	10	4	12.5	5	1
500	375	18	7	31.3	9	3
1000	750	30	11	62.5	13	4

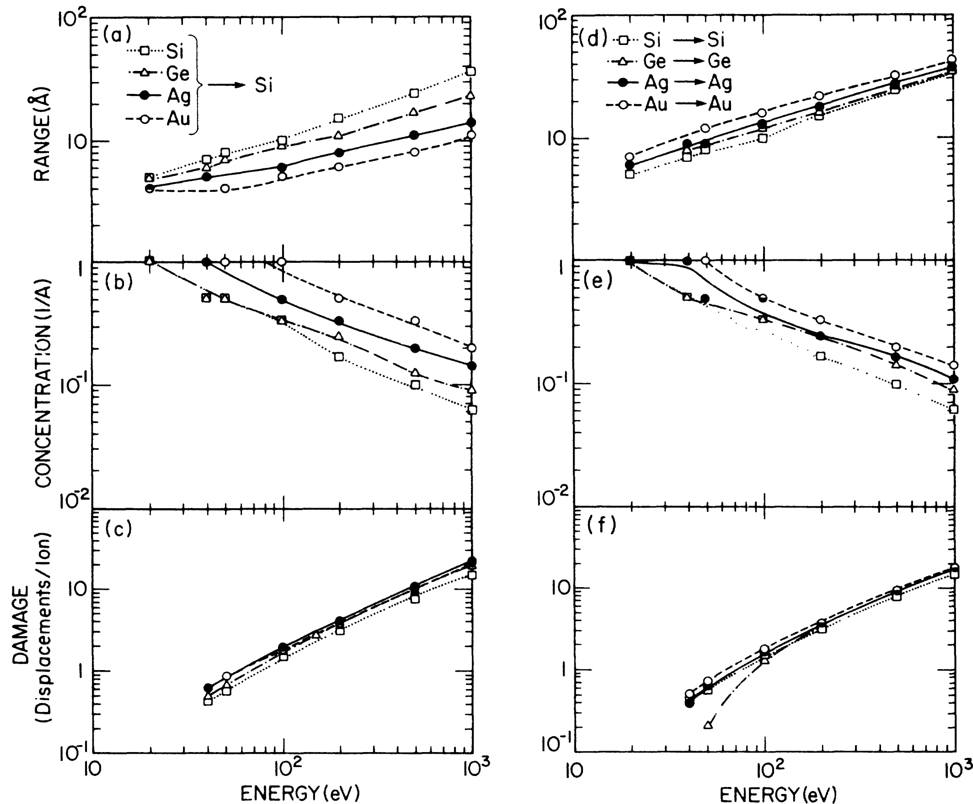

FIG. 13. TRIM calculations of hyperthermal ion bombardment of Si with Si, Ge, Ag, and Au 10-eV to 1-keV ions and of elemental targets with the same ions (Si→Si, Ge→Ge, Ag→Ag, and Au→Au). (a),(d) R_p; (b), (e) $1/\Delta R_p$; (c),(f) N_d. For bombardment of Si with different ions, increasing ion mass reduces the energy transferred to the Si atoms resulting in increasing R_p and decreasing local concentration. For bombardment of elemental targets with the same ions, the energy transferred in collision is the same for all cases resulting in a reversed mass effect (compared to bombardment on Si), i.e., higher R_p with increasing mass.

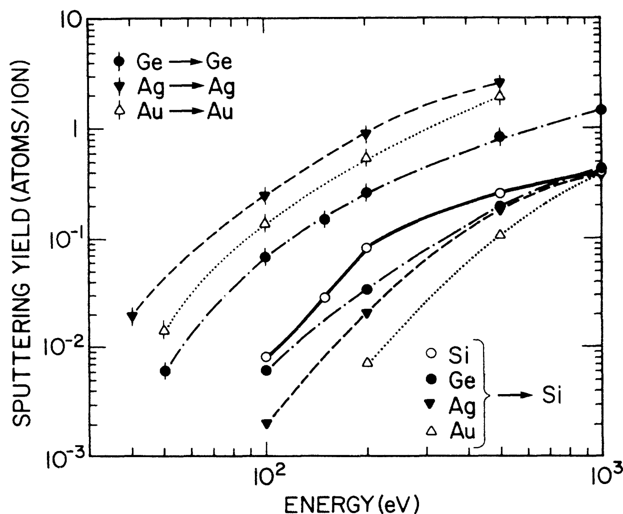

FIG. 14. TRIM calculations of S for different hyperthermal species impinging on different targets. Note low values for heavy ion bombardment on Si (smaller for higher mass) due to low-energy transfer and low Y_{BS}. Upon actual bombardment of M^+ on Si, the initial low value of S increases significantly as the pure M layer is evolving and eventually exceeds the values for Si^+ on Si.

Epitaxial growth of Si, Ge, and Ag from ion beams is different from that of diamond (the stable phase epitaxy is involved) and is more similar to that of graphite. The low-temperature epitaxy phenomena reported for these cases is generally explained in terms of "thermal spikes." We suggest that this epitaxy may be due to the subsurface nature of the process. When the temperature is low enough so that no significant diffusion of interstitials exists, amorphous films evolve due to the significant radiation damage, but a dense matrix is still formed. At elevated temperatures, interstitial migration to the surface occurs and some of the damage is annealed, resulting in a combination of surface layer-by-layer growth and subsurface bulk inclusion. Since it is diffusion from the bulk to the surface that occurs, surface processes that contribute to island formation and disordered film growth are suppressed and epitaxial growth is facilitated. In the equivalent system of $C^+ \rightarrow C$ at elevated temperatures, epitaxial growth of graphite, the stable carbon allotrope, occurs due to the migration of C interstitials to the surface. The "thermal-spike" model is not in accord with this temperature dependence of the epitaxial growth.

Further evidence for the subsurface nature of the processes involved is provided by reflection high-energy electron diffraction (RHEED) analysis of epitaxially grown Ag on Si that show transition from Ag-I (low-coverage

Ag) to Ag-II (high-coverage Ag) at much higher fluences than needed for a surface-monolayer transition.[64] Similarly, the reported low-temperature Si-Ge "alloying"[62] is consistent with subplantation and not low-temperature surface deposition. The defects observed in films deposited from low-energy ion beams are associated with two different phenomena: (i) radiation damage due to the impinging ions and (ii) dislocation loops associated with the spontaneous athermal process of formation of an inclusion of a new phase in an interstitial-rich region. A similar dislocation loop formation has been reported for high-dose He^+ implantation in solids.[45]

B. Ion-assisted deposition

In ion-assisted deposition, the main source for deposition is thermal species from an evaporation source or ~1–10-eV species sputtered from a target material. More energetic particles (~100–1000 eV) from another source simultaneously impinge on the evolving film. Beneficial modifications of the properties of various film have been reported,[1–3,5,6,8,9] including densification, formation of metastable phases, epitaxial or oriented growth at low temperatures, and stress relief. The following are several physical processes suggested to explain the data: (i) "thermal-spike" processes,[65] (ii) forward sputtering of atoms in a porous film,[1] and (iii) collisional processes.[23–28] Recent works[23–28] emphasize the role of displacements as the dominant effect for densification rather than "thermal spikes." The subplantation notations can be applied to ion-assisted deposition, but a separate analysis of the surface-deposition component as well as consideration of the synergistic effects of the two processes occurring simultaneously is needed. Nevertheless, preferential displacement of low-E_d atoms, leaving high-E_d atoms in their positions appears to be an important mechanism for densification and oriented growth of an initially porous, disordered media typical for thermally evaporated films.

V. CONCLUSIONS

(1) The subplantation model is capable of interpreting a large collection of data from carbon deposition from hyperthermal species as well as deposition of other materials.

(2) Two previous models for carbon deposition, "preferential sputtering" and "thermal spikes," do not provide explanations for the phenomena described in this paper.

(3) Additional experimental and theoretical work is needed. Future experimental work includes studies of both source and target parameters and establishment of relations between these parameters and film properties. Future theoretical work includes (i) improved trajectory calculations (both static and dynamic) that are capable of treating a crystalline rather than an amorphous material and different E_d's for the components of the evolving film, (ii) molecular-dynamic simulations treating many-body interactions and bonding, and (iii) atomistic calculations of the phase evolution of a subplanted material with a high concentration of interstitials.

(4) Of the various techniques that use hyperthermal species for deposition, MSIBD is unique in its ability to control the relevant deposition parameters within narrow, well-defined limits. This opens possibilities for both fundamental studies and deposition of films for practical purposes.

(5) Subplantation is a process that bridges the gap between ion implantation and surface deposition. Even at the present stage of understanding it offers promising possibilities (for fundamental science and technology) for carbon-film deposition as well as for other materials.

ACKNOWLEDGMENTS

The authors would like to express their gratitude to O. Grizzi and D. Marton for helpful discussions and a critical review of the manuscript and to J. F. Ziegler for providing the IBM computer version of the TRIM program. This material is based on work supported by the National Science Foundation under Grant No. DMR-86-10597 and the R. A. Welch Foundation (Houston, TX) under Grant No. E656.

*Present address: Soreq Nuclear Research Center, 70600 Yavne, Israel.
†Present address: IBM Research Division, Thomas J. Watson Research Center, P.O. Box 218, Yorktown Heights, NY 10598.

[1] J. M. E. Harper, J. J. Cuomo, R. J. Gambino, H. R. Kaufman, in *Ion Bombardment Modification of Surfaces: Fundamentals and Applications,* edited by O. Auciello and R. Kelly (Elsevier, Amsterdam, 1987), Chap. 4.
[2] C. Weissmantel, in *Thin Films From Free Atoms and Particles,* edited by K. J. Klabunde (Academic, Orlando, Florida, 1985), Chap. 4.
[3] G. Gautherin, D. Bouchier, C. Schwebel, in *Thin Films From Free Atoms and Particles,* edited by K. J. Klabunde (Academic, Orlando, Florida, 1985), Chap. 5.
[4] J. C. Angus, P. Koidl, and S. Domitz, in *Plasma Deposited Thin Films,* edited by J. Mort and F. Jansen (CRC, Boca Raton, Florida, 1986), Chap. 4.
[5] J. E. Greene, T. Motooka, J. E. Sundgren, D. Lubben, S. Gorbatkin, and S. A. Barnett, Nucl. Instrum. Methods Phys. Res. B **27**, 226 (1987).
[6] T. Takagi, Thin Solid Films **92**, 1 (1982); T. Takagi, J. Vac. Sci. Technol. A **2**, 382 (1984).
[7] R. A. Zuhr, S. J. Pennycook, T. S. Noggle, N. Herbots, T. E. Haynes, and B. R. Appleton, Nucl. Instrum. Methods Phys. Res. B **37/38**, 16 (1989).
[8] P. J. Martin, J. Mater. Sci. **21**, 1 (1986).
[9] S. M. Rossnagel and J. J. Cuomo, Vacuum **38**, 73 (1988).
[10] H. Tsai and D. B. Bogi, J. Vac. Sci. Technol. A **5**, 3287 (1987).
[11] J. C. Angus and C. C. Hayman, Science **241**, 913 (1988).
[12] Y. Lifshitz, S. R. Kasi, and J. W. Rabalais, Adv. Mater. Manu. Process. **3**, 157 (1988).
[13] S. R. Kasi, Y. Lifshitz, and J. W. Rabalais, Angew. Chem., Adv. Mater. **100**, 1245 (1988).

[14]S. Aisenberg and R. Chabot, J. Appl. Phys. **42**, 2953 (1971).

[15]*The Properties of Diamond,* edited by J. E. Field (Academic, London, 1979).

[16]*Plasma Deposited Thin Films* (Ref. 4), pp. 96 and 97; Thin Solid Films **92**, 338 (1982). *Ion Bombardment Modification of Surfaces: Fundamentals and Applications* (Ref. 1), p. 159.

[17]E. G. Spencer, P. H. Schmidt, D. C. Joy, and F. J. Sansalone, Appl Phys. Lett. **29**, 118 (1976).

[18]F. Seitz and J. S. Koehler, *Progress in Solid State Physics* (Academic, New York, 1957), Vol. 12, p. 10.

[19]C. Weissmantel, Thin Solid Films **92**, 55 (1982).

[20]C. G. Gilmore, A. Haeri, and J. A. Sprague, in *Materials Research Society Symposium Proceedings* (MRS, Pittsburgh, 1989), Vol. 128, p. 163.

[21]G. E. Thomas, L. J. Beckers, J. J. Vrakking, and B. R. de Koning, Cryst. Growth **56**, 557 (1982).

[22]N. Herbots, B. R. Appleton, T. S. Noggle, R. A. Zuhr, and S. T. Pennycook, Nucl. Instrum. Methods Phys. Res. B **13**, 250 (1986).

[23]K. H. Müller, J. Appl. Phys. **59**, 2803 (1986).

[24]K. H. Müller, Surf. Sci. **184**, L375 (1987).

[25]K. H. Müller, J. Appl. Phys. **62**, 1796 (1987).

[26]D. R. Brighton and G. K. Hubler, Nucl. Instrum. Methods Phys. Res. B **28**, 527 (1987).

[27]G. I. Grigorov, I. Martev, J. P. Langeron, and J. L. Vignes, Thin Solid Films **161**, 249 (1988).

[28]B. W. Dodson, in *Materials Research Society Symposium Proceedings* (MRS, Pittsburgh, 1989), Vol. 128, p. 137.

[29]Y. Lifshitz, S. R. Kasi, and J. W. Rabalais, Phys. Rev. Lett. **62**, 1290 (1989).

[30]J. F. Ziegler, J. P. Biersack, and U. Littmark, *The Stopping and Ranges of Ions in Matter* (Pergamon, Oxford, 1985), Vol. 1.

[31]J. P. Biersack and W. Eckstein, Appl. Phys. A **34**, 73 (1984);

[32]S. R. Kasi, H. Kang, and J. W. Rabalais, J. Chem. Phys. **88**, 5914 (1988).

[33]G. Dearnaley *et al.*, *Ion Implantation* (North-Holland, Amsterdam, 1973), p. 155.

[34](a) W. Möller, and W. Eckstein, Nucl. Instrum. Methods Phys. Res. B **2**, 814 (1984); (b) W. Möller, W. Eckstein, and J. P. Biersack, Comput. Phys. Commun. **51**, 355 (1988).

[35]L. C. Feldman, and J. W. Mayer, *Fundamentals of Surface and Thin Film Analysis* (Elsevier, New York, 1986), Chap. 6.

[36]G. E. Rhead, M. G. Barthes, and C. Argile, Thin Solid Films **82**, 201 (1981).

[37]K. Reichelt, Vacuum **38**, 1083 (1988).

[38]H. H. Andersen and H. L. Bay, in *Sputtering by Particle Bombardment I,* edited by R. Behrisch (Springer-Verlag, New York, 1981), Chap. 4.

[39]E. A. Burgermeister, C. A. J. Ammerlaan, and G. Davies, J. Phys. C **13**, L691 (1980).

[40]E. F. Chaikovskii, V. M. Puzikov, and A. V. Semenov, Kristallografiya **26**, 219 (1981) [Sov. Phys.—Crystallogr. **26**, 122 (1981)].

[41]J. Ishikawa, Y. Takeiri, K. Ogawa, and T. Takagi, Nucl. Instrum Methods Phys. Res. B **21**, 205 (1987).

[42]T. Miyazawa, S. Misawa, S. Yoshida, and S. Gonda, J. Appl. Phys. **55**, 188 (1984).

[43]H. Ullmaier, Radiat. Eff. **78**, 1 (1983).

[44]W. D. Wilson, Radiat. Eff. **78**, 11 (1983).

[45]H. H. Madden and J. E. Houston, J. Vac. Sci. Technol. **14**, 412 (1977).

[46]R. E. Clausig, D. S. Easton, and G. L. Powell, Surf. Sci. **36**, 377 (1973).

[47]J. H. Freeman, W. Temple, and G. A. Gard, Vacuum **34**, 305 (1984).

[48]E. F. Chaikovskii and G. Kh. Rozenberg, Dokl. Akad. Nauk SSSR **279**, 1372 (1984) [Sov. Phys.—Dokl. **29**, 1043 (1984)].

[49]E. F. Chaikovskii *et al.*, Archinum Nauki O Matrialach t. **7,2,2**, 187 (1986) (in Russian).

[50]J. F. Prins, Phys. Rev. B **31**, 2472 (1985).

[51]J. F. Prins, Radiat. Eff. Lett. **76**, 79 (1983).

[52]J. F. Prins, T. E. Derry, and J. P. F. Sellschop, Phys. Rev. B **34**, 8870 (1986).

[53]R. S. Nelson, J. A. Hudson, D. J. Mazey, and R. C. Piller, Proc. R. Soc. London, Ser. A **386**, 211 (1983).

[54]J. Koskinen, J. P. Hirvonen, and A. Anttila, Appl. Phys. Lett. **47**, 941 (1985).

[55]J. Ishikawa, Y. Takeiri, K. Ogawa, and T. Takagi, J. Appl. Phys. **61**, 2509 (1987).

[56]M. Kitabatake and K. Wasa, J. Appl. Phys. **58**, 1693 (1985).

[57]S. R. Kasi, H. Kang, C. S. Sass, and J. W. Rabalais, Surf. Sci. Rep. **10**, 1 (1988).

[58]K. Kobashi, K. Nishimura, Y. Kawate, and T. Horiuchi, Phys. Rev. B **38**, 4076 (1988).

[59]W. L. Hsu, J. Vac. Sci. Technol. A **6**, 1807 (1988).

[60]B. R. Appleton, R. A. Zuhr, T. S. Noggle, N. Herbots, and S. J. Pennycook in *Materials Research Society Symposium Proceedings* (MRS, Pittsburgh, 1987), Vol. 74, p. 45.

[61]R. A. Zuhr, B. R. Appleton, N. Herbots, B. C. Larson, T. S. Noggle, and S. J. Pennycook, J. Vac. Sci. Technol. A **5**, 2135 (1987).

[62]K. Miyake and T. Tokuyama, Thin Solid Films, **92**, 123 (1982).

[63]P. C. Zalm and L. J. Beckers, Appl. Phys. Lett. **41**, 167 (1982).

[64]J. J. Vrakking, L. J. Beckers, and G. E. Thomas, Thin Solid Films **92**, 131 (1982).

[65]E. H. Hirsch and I. K. Varga, Thin Solid Films **69**, 99 (1980).